JOURNAL OF GEOPHYSICAL RESEARCH, VOL. 105, NO. D4, PAGES 4979-4991, FEBRUARY 27, 2000

Simulation of mineral dust effects on UV radiation levels

Juan P. Díaz, Francisco J. Expósito, Carlos J. Torres, and Virgilio Carreño
Department of Physics, University of La Laguna, Santa Cruz de Tenerife, Canary Islands, Spain

A. Redondas
Instituto Nacional de Meteorología, Santa Cruz de Tenerife, Canary Islands, Spain

Abstract. The role played by aerosols on UV radiative transfer in the atmosphere is very uncertain. This is especially true regarding mineral dust. To determine the sensitivity of the UV levels to the presence of this atmospheric specie, we have simulated the UV irradiance with different vertical distributions of mineral dust. We have used a discrete ordinates radiative transfer model to obtain the UV levels both at sea level and at 3000 m. We have computed the aerosol single-scattering albedo, the phase function, and the asymmetry factor by Mie scattering theory. The background aerosol profiles were taken from *WCRP* [1986] models, whereas the radiative properties of mineral dust have been calculated from the aerosol size distribution obtained during Saharan dust invasions at Tenerife island (28.5°N, 16.3°W). The values for aerosol optical depth assumed as input for the model calculations are 0.2 (at 550 nm) for clean background aerosols and 0.3 (at 550 nm) for the mineral dust component. From the results we can conclude that the dust vertical size distribution can affect the irradiance ratio F (with Saharan dust)/F (no Saharan dust) by 2-4%. In addition, we observe that to the same total optical depth the diffuse UV levels depend not only on the vertical dust distribution but also on the background aerosol vertical distribution. We have computed differences for the diffuse radiation fluxes of about 5% between a maritime and a continental model to the same mineral dust vertical distribution.

1. Introduction

Atmospheric aerosols modify the energy balance in the Earth-atmosphere system and also the UV radiation levels at the surface. This component can affect climate both directly, by radiation scattering and absorption, and indirectly, producing changes in the cloud droplet concentration and size distribution.

The role played by aerosols on the UV radiative transfer in the atmosphere is very uncertain. It is necessary to decrease this uncertainty in order to improve the modeling of the energy transfer due to the important role played by UV radiation in the biosphere.

Early studies about the influence of aerosols in the Earth-atmosphere system energy budget has been mainly centered on particles from anthropogenic sources, such us non-sea-salt sulfate (nss $SO_4^=$), aerosols from biomass burning, etc. They have shown that the effect of these compounds is comparable to greenhouse effect gases but opposite in sign. For example, *Kiehl and Briegleb* [1993] and *Taylor and Penner* [1994] suggest a global average direct radiative forcing (ΔF) in the range of ΔF = -0.3 and -0.9 W/m^2. For biomass burning aerosols, *Penner et al.* [1992] estimate a direct radiative forcing around -1 W/m^2.

Nevertheless, recent studies have pointed out the importance of the mineral dust in the determination of the atmospheric radiative properties, mainly in the oceanic regions where this is the dominant aerosol component.

Modeling studies indicate that the directly radiative forcing by mineral dust could be significant on a global scale and dominant on regional scales. Authors such us *Tegen et al.* [1996] propose a value of -1 W/m^2, whereas *Sokolik and Toon* [1996] have estimated a mineral dust forcing of about -0.25 W/m^2 over land and -0.6 W/m^2 over oceans.

On the other hand, *Tegen and Lacis* [1996] have shown that the mineral dust radiative forcing depends on the vertical distribution of this atmospheric constituent. These authors have pointed out that the changes in the tropospheric radiation levels are a function of the effective radius of the aerosol distribution for different vertical distributions.

Herman et al. [1997] have studied the distribution of the UV-absorbing aerosols by radiance differences between the 340 and the 380 nm channels from the Nimbus 7 Total Ozone Mapping Spectrometer (TOMS). They have shown that a significant portion at the Earth surface is covered by UV-absorbing aerosols (biomass burning and desert dust) 11 months of the year.

In this work we study the mineral dust because this is the aerosol species which radiative properties presents the greater uncertainties, not only in the UV region but also in the VIS-IR zone. Thus this paper follows two goals: (1) to determine the sensitivity of the UV radiation levels as a function of the vertical profiles of the mineral dust concentrations and (2) to study the variation of the UV radiation levels to different standard aerosol with the presence of mineral dust.

Section 1 of this work describes the methodology used to characterize the radiative properties of desert aerosols. Section

Paper number 1999JD901058.
0148-0227/00/1999JD901058$09.00

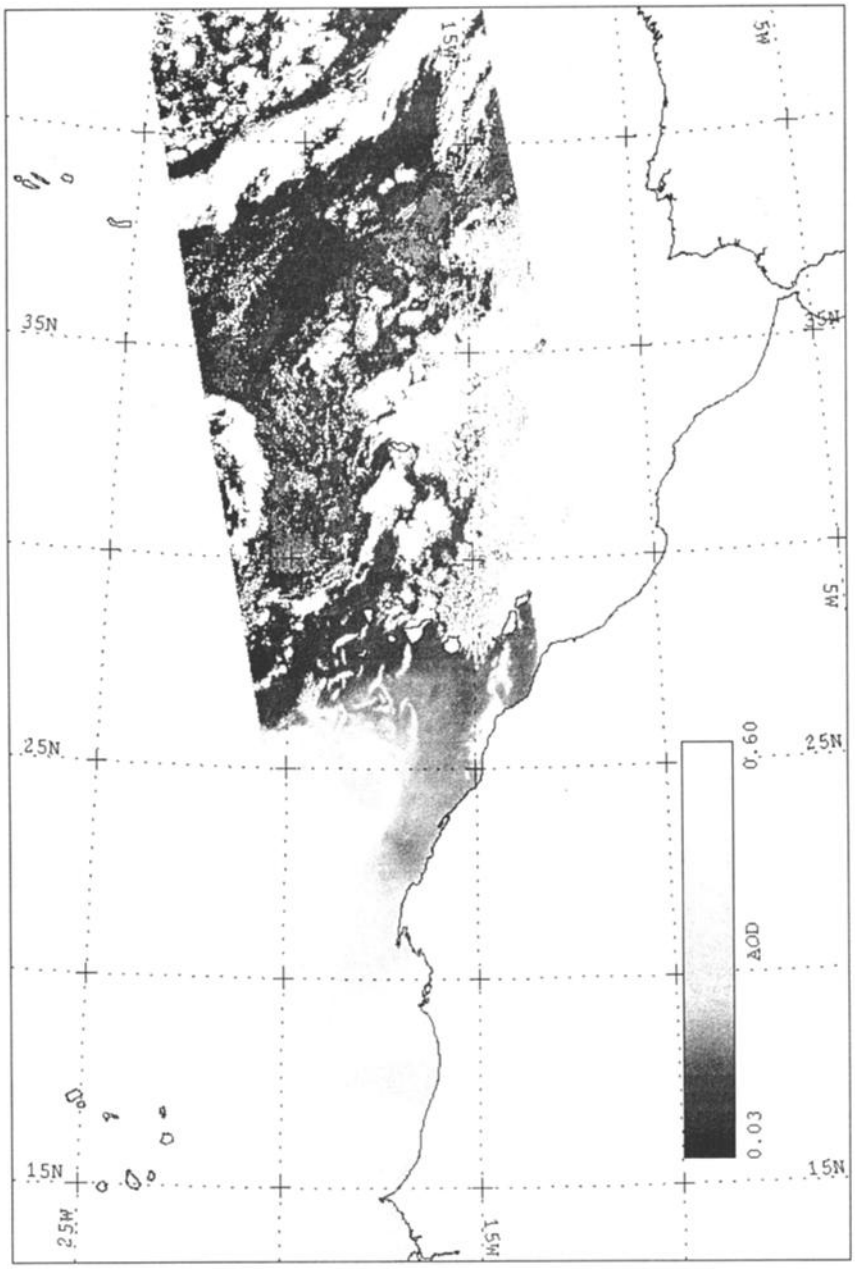

Figure 1. Aerosol optical depth (AOD) computed from the radiance levels of the AVHRR/NOAA-11 channel 1. The lightest image pixels correspond to the higher dust concentrations.

2 shows the radiative transfer model employed and the scheme followed to model the real atmosphere. The mineral dust vertical distribution has been implemented by three different patterns: in the first one the mineral dust is introduced between 0 and 3 km, in the second one between 3 and 6 km, and in the last one between 0 and 6 km. Finally, we have compared the UV irradiance levels at surface with different aerosol vertical size distributions with the presence of mineral dust.

2. Model of Mineral Dust

2.1. Aerosol Optical Depth and Size Distributions

To determine the radiative properties of the atmospheric aerosols, we have measured the aerosol optical depth to the wavelengths of 368.0, 500.0, and 778.0 nm. For this we have used a PMOD/WRC Sun photometer located at the Izaña Global Atmospheric Watch Station, Tenerife, Canary Islands (28.5°N, 16.3°W). This region is ideally suited for the study of radiative effects of dust because it experiences frequent African dust events, especially during the summer and early fall [*Arimoto et al.*, 1995; *Prospero*, 1996a, b]. The desert dust can arrive at this region in the marine boundary layer (MBL) or in the so-called Saharan air layer (SAL), which has its top at a height of 6 km. Frequently, the dust concentration in the SAL is several times superior to the one detected in the MBL [*Prospero*, 1996a]. The major sources of mineral dust are in the African NW (Saharan desert and Sahel region) which present a seasonal behavior in its strength. The dust outbreaks in this region are usually observable from space platforms. In

Figure 1 we can see an aerosol optical depth (AOD) image computed from the radiance levels of AVHRR/NOAA-11 channel 1, where the dust outbreak is clear. This product has been evaluated by the linearized single-scattering approximation (LSSA) described by *Expósito et al.* [1997] and *Porter* [1993].

To calculate the AOD from ground radiance measurements, we have used the Lambert-Beer-Bouguer law, which can be written as

$$L(\lambda) = \frac{L_0(\lambda)}{S_0} \exp\left(-\left[\tau_R + \tau_{abs} + \tau_A\right]\delta\right), \quad (1)$$

where $L(\lambda)$ is the monochromatic radiance to the wavelength λ, $L_0(\lambda)$ is the radiance measured by the instrument outside the Earth's atmosphere to the Sun-Earth mean distance (exoatmospheric constant), τ_R is the Rayleigh optical depth, τ_{abs} is the optical depth due to the absorption gases at λ, τ_A is the aerosol optical depth, δ is the air mass, and S_0 is a factor that corrects the exoatmospheric constant to the actual Earth-Sun distance. The factors τ_R and δ have been evaluated using the following expressions [*WMO*, 1980; *Iqbal*, 1983]:

$$\delta = \left[\cos\theta_0 + 0.15\cdot(93.885 - \theta_0)^{-1.263}\right]^{-1}, \quad (2)$$

$$\tau_R = 0.00838\lambda^{-(3.916+0.074\lambda-0.05/\lambda)}, \quad (3)$$

where θ_0 is the solar zenith angle, and λ is given in microns. We have used the correction factor P(mbar)/1013.25 [*Iqbal*, 1983] to correct by height. Following *Russell et al.* [1993] and *Dutton et al.* [1994] we have considered the same air mass for all terms in the exponent of equation (1), i.e., molecules, absorbing gases, and aerosols. This approximation is fine when the measurements are done with solar zenith angles less than 60°. The only absorbing gas taken into account is the ozone (Chappuis band) at 500 nm. The O_3 absorption optical depth has been evaluated by the expression

$$\tau_{abs} = \sigma(\lambda)C_{Oz}, \quad (4)$$

where σ(500 nm) = 0.034 cm^{-1} is the absorption cross section and C_{Oz} is the total ozone concentration. A Brewer instrument located at the Izaña Global Atmospheric Watch (GAW) Station has measured this last quantity.

Interference filters select the three channels of the PMOD/WRC Sun photometer (368, 500, and 778 nm) with a full width at half maximum (FWHM) of 5 nm. The collimated tube of this instrument has a field of view (FOV) of 2.6° and is installed in a Sun tracker, which permits an automatic and precise alignment with the Sun. Although the equipment works automatically, an observer inspects it daily for verification of proper operation. To minimize the possible variations in the response of the instrument sensors due to thermal changes, the cavity where they are located is thermostatized at 30°C. The detector is a silicon photovoltaic sensor type UV-215B.

The radiance $L_0(\lambda)$ has been obtained by Langley plot calibration made at Izaña station for days with high atmospheric stability. This calibration is done by the representation of the natural logarithm of radiation intensity versus air mass. From this slope it is possible to obtain the total optical depth, whereas the extrapolation to air mass zero gives us the exoatmospheric constant. The correlation coefficients for the linear regressions of these calibrations have always been greater than 99.9% with a fit standard deviation less than 0.002 [*Díaz et al.*, 1994]. The exoatmospheric values obtained in this way have been compared with those obtained by Herman's method [*Herman et al.*, 1981]. This algorithm does a statistical treatment of the radiance data in the hypothesis that the necessary atmospheric stability breaks due to random fluctuations in the optical depth values. The differences between the results of both methods are less than 1% at each of the three wavelengths used.

The principal error sources in the AOD values are as follows: air mass determination, accuracy characterization of the transmission curve of the interference filters, the circumsolar radiation, which is detected by the radiometer due to its finite FOV, and the calculation of the exoatmospheric constant. Taking into account these error sources and the works of *Russell et al.* [1993], *Dutton et al.* [1994], *Thomason et al.* [1983], *Reagan et al.* [1986], and *Box and Deepak* [1979], the error in the AOD values ranges between $\Delta\tau_A = \pm 0.013$ in channel 1 (368 nm) and $\Delta\tau_A = \pm 0.003$ in channel 3 (778 nm).

The particle size distribution has been computed from the aerosol optical depth using the constrained inversion method of *King et al.* [1978] (see Figure 2). The aerosol optical depth is related to particle size distribution in the atmospheric column, $n(r) = \int n(r,z)dz$, through the Fredholm integral equation of the first kind (equation (5)):

$$\tau_A(\lambda) = \int_0^\infty \pi r^2 Q_{ext}(\lambda,r,m)n(r)dr, \quad (5)$$

where $Q_{ext}(\lambda,r,m)$ is the extinction efficiency factor, which depends on the wavelength λ, the particle radii r, and the refraction index m. $Q_{ext}(\lambda,r,m)$ has been computed by the algorithm of *Wiscombe* [1980], which has an accuracy of at least six significant digits. *King et al.* [1978] and *Amato et al.* [1988] have noted that the problem of determining the aerosol size distribution by equation (5) is ill posed. To guarantee the convergence of the method, it is very important to choose properly the radii interval where equation (5) is going to be applied. In this work we have used the *Heintzenberg et al.* [1981] criteria. This procedure establishes that the particle radii interval where the inversion method can be applied is given by the condition that the ratio between the efficiency factor computed to different wavelengths depends on the particle radii. Three wavelengths are the minimum information set necessary to obtain aerosol size distribution by the King's inversion method. *Dutton et al.* [1994] have satisfactorily used the same three wavelengths (368, 500, and 778 nm) to study the radiative characteristic of the aerosols at Mauna Loa, Hawaii.

The data goodness obtained by the King's inversion method has been tested as follows: Using the aerosol vertical profiles published by *WCRP* [1986], we have computed the total aerosol size distribution in the atmospheric column. To simulate the presence of mineral dust we have increased the total particle number in the coarse mode following a lognormal distribution to several optical depth values [*Longtin et al.*, 1988]. To these "real" size distributions we have computed the AOD, the single-scattering phase function ($P(\Theta)$, equation (6)), the asymmetry factor (g, equation (7)), and the single-scattering albedo (ω, equation (8)) to 368, 500, and 778 nm, using a refraction index that depends on wavelength [*WCRP*, 1986]. From these three AOD values we

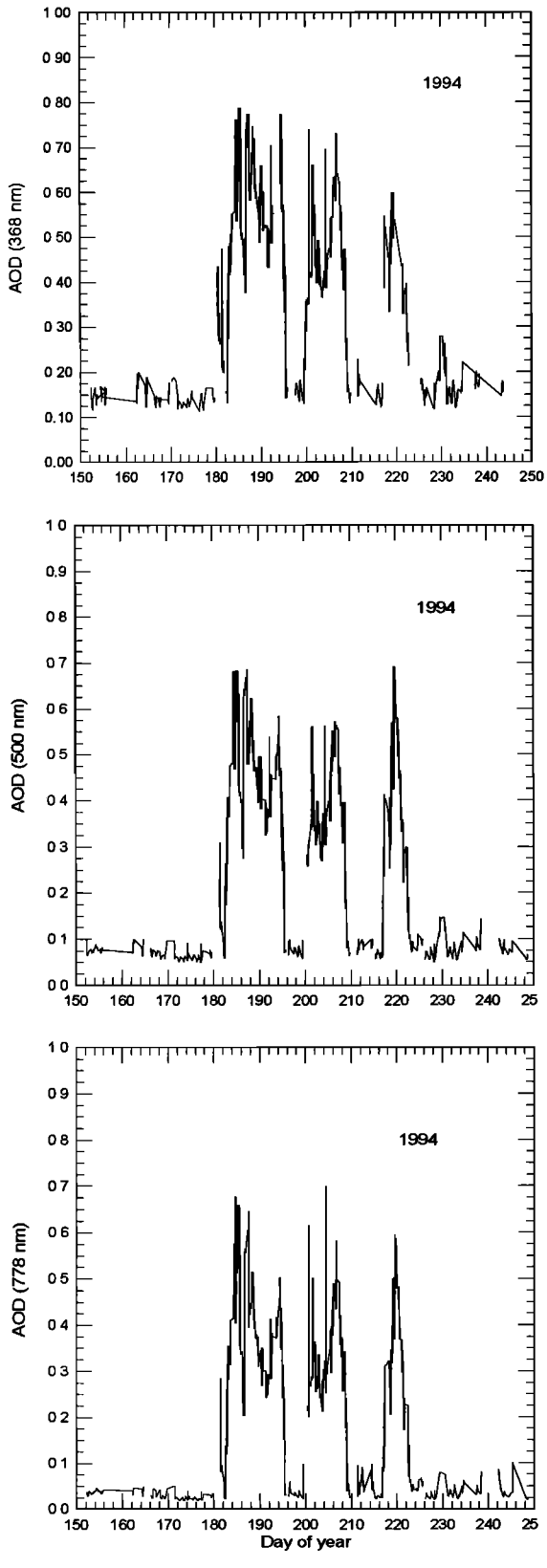

Figure 2. Aerosol optical depth obtained at the Izaña Global Atmospheric Watch (GAW) Station.

have recalculated the aerosol size distribution ($n(3\lambda)$) using King's method. With $n(3\lambda)$ we have recomputed $g(3\lambda)$, $\omega(3\lambda)$, and $P(3\lambda)$. Note that in the implementation of King's procedure the refraction index must be constant with the wavelength, and it has been fixed to 1.570-0.006*i* [*Patterson et al.*, 1978].

Table 1 shows the values of g and ω for the case of a MAR-I particle vertical distribution [*WCRP*, 1986] with $\tau_A = 0.2$ and for other two cases with the addition of mineral dust to produce AOD values of $\tau_A = 0.5$ and $\tau_A = 1.0$. The results show that the discrepancies for g and ω increase with the AOD. Both at 300 and 400 nm the uncertainties for g do not exceed 7%, whereas for ω at 300 nm, the maximum errors are about 10% and at 400 nm about 8% in all the cases studied. These results show that the radiative properties can be obtained, although the errors in the complex refraction index are considerable. For the single-scattering aerosol phase function the maximum errors are in the backscattering zone and also increase with AOD. In the worst case the uncertainties are around 30% (see Figure 3).

2.2. Mineral Dust Radiative Properties

From the particle size distributions obtained with the presence of mineral dust at the Izaña station we have computed the mineral dust radiative properties. The radiative transfer computer code used (DISORT [*Stamnes et al.*, 1988]) characterizes the aerosols by the single-scattering aerosol phase function ($P(\Theta)$), the asymmetry factor (g), and the single-scattering albedo (ω):

$$P(\Theta) = \frac{4\pi}{2k^2\sigma_S}\left(|S_1|^2 + |S_2|^2\right), \tag{6}$$

$$g = \frac{\int_0^\infty \pi r^2 Q_{\text{sct}}(\lambda, r, m) g'(\lambda, r, m) n(r) dr}{\int_0^\infty \pi r^2 Q_{\text{sct}}(\lambda, r, m) n(r) dr}, \tag{7}$$

$$\omega = \frac{\int_0^\infty \pi r^2 Q_{\text{sct}}(\lambda, r, m) n(r) dr}{\int_0^\infty \pi r^2 Q_{\text{ext}}(\lambda, r, m) n(r) dr}, \tag{8}$$

where g' is the asymmetry factor for a single particle of radium r and refraction index m, k is the wave number, σ_S is the scattering cross section, and S_1 and S_2 are the scattering functions. Q_{sct}, Q_{ext}, g', S_1, and S_2 have been evaluated using the *Wiscombe* [1980] algorithm.

The two main error sources in the parameters $P(\Theta)$, g, and ω calculated from the aerosol size distribution obtained through the nonparametric King's inversion method are the nonsphericity of the particles (and thus the nonvalidity of the Mie theory) and the variation in the refraction index with λ.

Different authors such us *Mishchenko et al.* [1997], *West et al.* [1997], or *Kahn et al.* [1997] have studied the possible

Table 1. Asymmetry Factor and Single-Scattering Albedo Comparison Obtained From a Real and a Three Wavelength Modeled Aerosol Size Distribution

	300 nm	300 nm	400 nm	400 nm
	g real, $g(3\lambda)$	ω real, $\omega(3\lambda)$	g real, $g(3\lambda)$	ω real, $\omega(3\lambda)$
$\tau = 0.2$	0.683. 0.687	0.890, 0.927	0.695, 0.651	0.890, 0.938
$\tau = 0.5$	0.772, 0.808	0.816, 0.790	0.746, 0.770	0.860, 0.854
$\tau = 1.0$	0.811, 0.864	0.789, 0.699	0.762, 0.816	0.852, 0.780

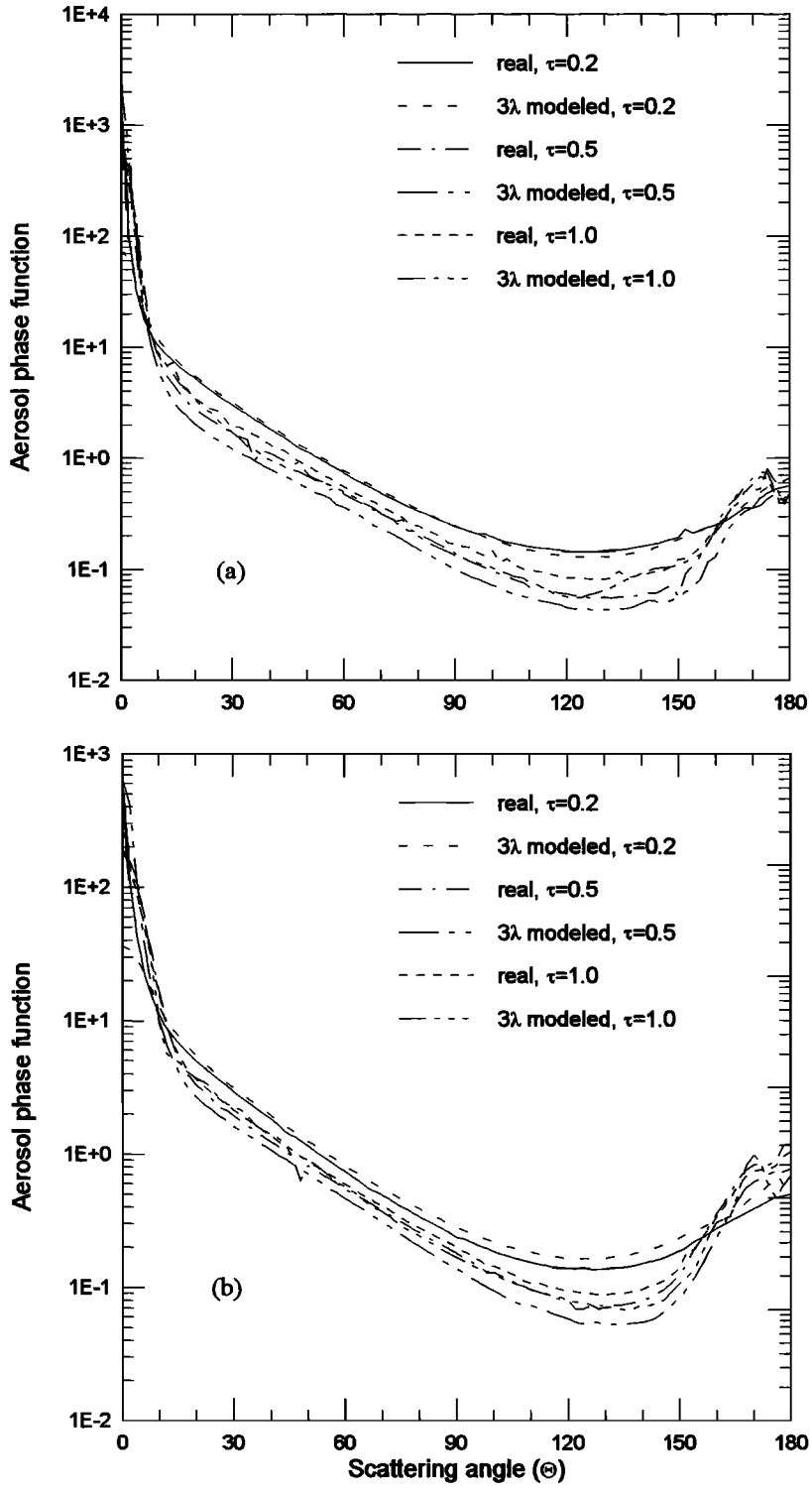

Figure 3. Aerosol single-scattering phase function obtained by a real size distribution and a three wavelength modeled aerosol size distribution: (a) 300 and (b) 400 nm.

invalidity of Mie theory. In those works the error in the main mineral dust radiative properties has been studied comparing values obtained to spherical particles with those computed for several sets of particle shapes, both theoretically and experimentally. For the smallest particles, i.e., particles with effective radii less than 0.5 μm, the phase functions are indistinguishable. For distributions with effective radii between 0.5 and 10.0 μm, which correspond to typical values of suspended atmospheric mineral dust aerosols, the differences could be important. For these larger aerosols the nonspherical particles put a smaller fraction of the total scattering into the backscattering direction at scattering angles greater than about 150° and a larger fraction into the scattering angles between about 100° and 150° compared to spherical

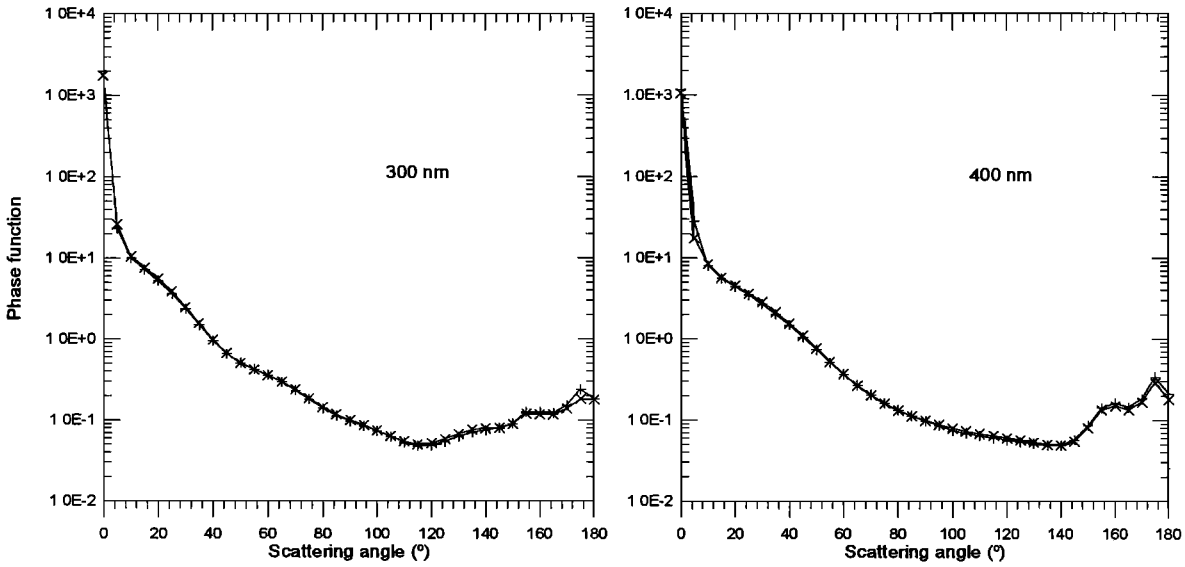

Figure 4. Phase function to dusty condition obtained by expression (6).

particles with an equivalent surface area. Nevertheless, these authors have established that the differences are especially small in the single-scattering albedo for a size parameter greater than 1. For size parameters greater than 2 these errors do not exceed 2%. On the other hand, the differences between sphericity and nonsphericity to the asymmetry factor are less than 7% for the size parameter range from 0 to 30 and less than 3.5% for size parameters larger than 7. Anyway, the results found by *Mishchenko et al.* [1997], *Lacis and Mishchenko* [1995], and *Mishchenko et al.* [1995] suggest that the influence of the particle shape in the aerosol radiative forcing can be considered negligibly small. Thus they can be accurately computed using the Mie theory if the AOD is already known, such as it happens in this work.

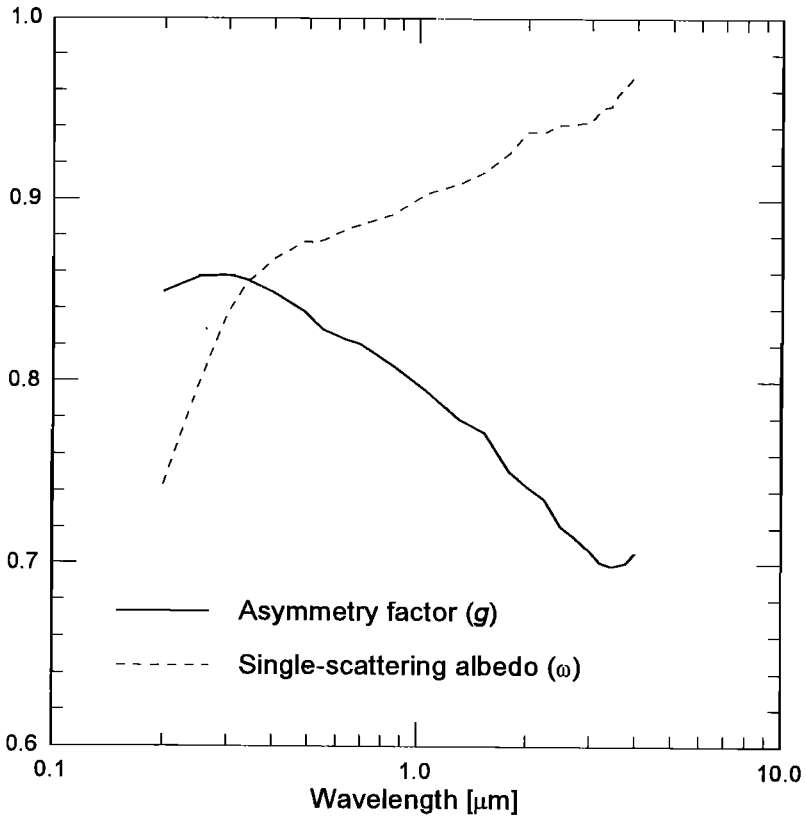

Figure 5. (Solid curve) Asymmetry factor g averaged for all dusty days versus λ and (dashed curve) single-scattering albedo ω averaged for all dusty days versus λ.

González-Jorge and Ogren [1996] and *Amato et al.* [1988] have studied the uncertainties in the asymmetry factor and in the single-scattering albedo due to the error propagation in the refractive index values. These authors have also used the nonparametric King's inversion method to model the aerosol size distributions. If a constant refraction index is used, the error in g is less than 8%.

We have calculated the aerosol phase function, the asymmetry factor, and the single-scattering albedo from the aerosol size distribution obtained under Saharan dust invasions at the Izaña GAW Station using equations (6)-(8). In Figure 4 we show $P(\Theta)$ values for the wavelengths of 300 and 400 nm during Julian days 180 and 182 (June 29 and July 1, 1998), whereas Figure 5 shows the averaged values of $g(\lambda)$ and $\omega(\lambda)$ in the solar spectrum using the values obtained in those days in which the dust was detected over the station.

For all the days where the mineral dust was detected the studied radiative properties were fairly constant. So we can see that the phase function does not change from day to day, and the average asymmetry factor and the average single-scattering albedo both show standard deviations less than 4% and 2%, respectively, for the wavelength total set shown in Figure 5.

3. Atmospheric and Radiative Transfer Model

To carry out the proposed goals, we have used the radiative transfer computer code DISORT [*Stamnes et al.*, 1988], which is a discrete ordinates radiative transfer model. This algorithm includes multiple scattering in a vertically inhomogeneous nonisothermal plane-parallel media, and it has been shown to be computationally efficient and reliable to resolve the radiative transfer equation (RTE). The Earth's atmosphere is constituted by a set of radiatively active gases and particles with variable concentrations in height. To model this real situation, the atmosphere has been divided in 20 layers following the Forster scheme [*Forster*, 1995]. The radiative properties of aerosols and absorbing gases are considered constant within each layer but are allowed to change from one layer to the next. The variables defined in each layer are: the single-scattering albedo, the aerosol phase function (given by its expansion in a Legendre polynomial series), and the total optical depth (TOD). To calculate TOD, the Rayleigh optical depth has been evaluated by the *WMO* [1980] expression, pressure corrected.

To study the variation of the radiation levels as a function of the mineral dust vertical distribution, we have used the following scheme. It has been established a clean background

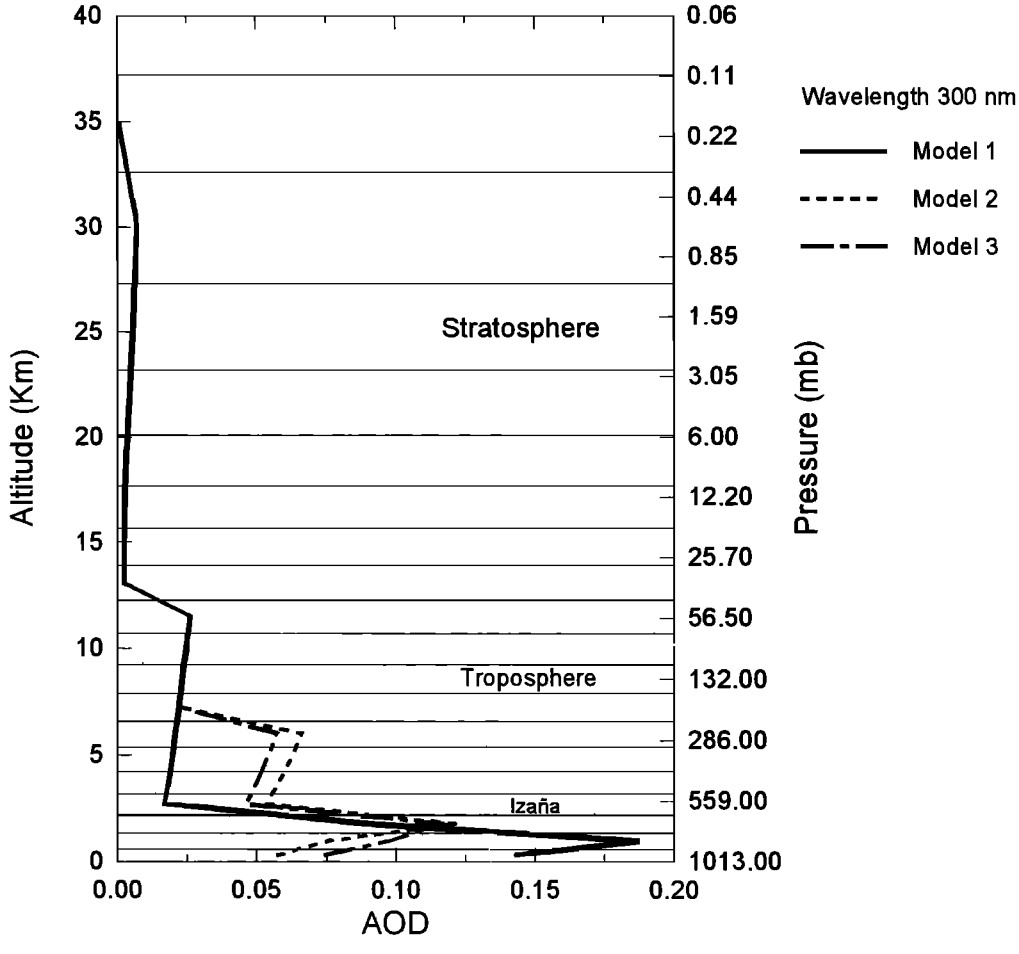

Figure 6. Scheme of the atmospheric layers considered in the model. Note that on the x axis is plotted AOD per layer. Model 1 corresponds to the situation in which the dust is concentrated below the thermal inversion layer (TIL). For model 2 the dust is located between TIL and the Saharan air layer (SAL), and in model 3 the dust is distributed between the top of the SAL and the sea level.

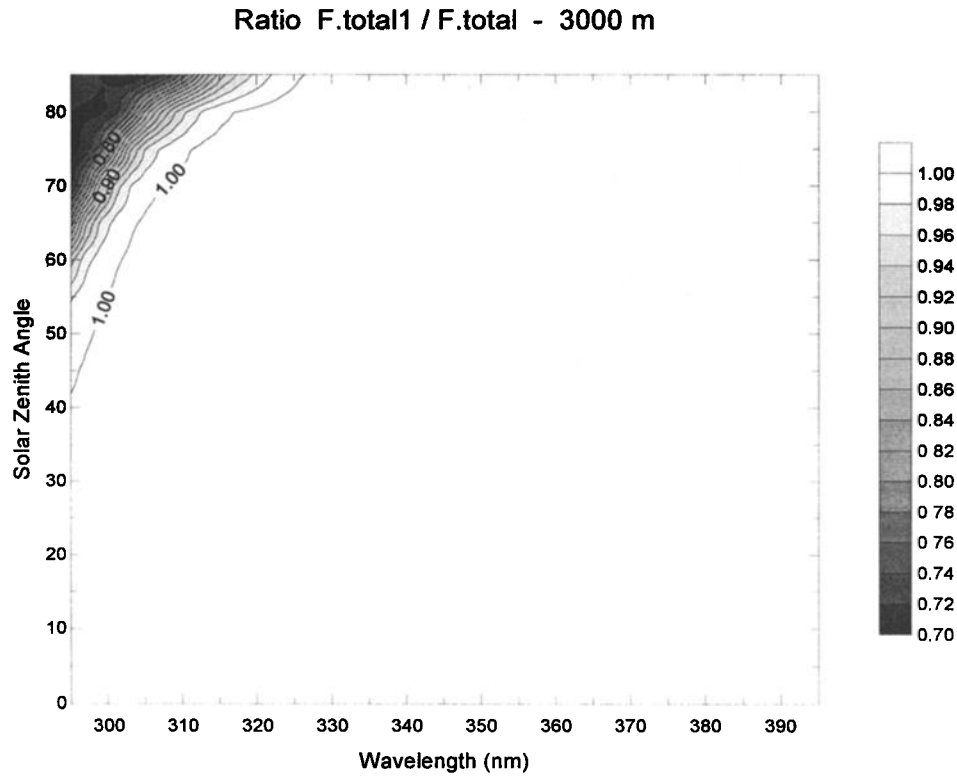

Figure 7a. Total irradiance ratio at 3000 m for case 1.

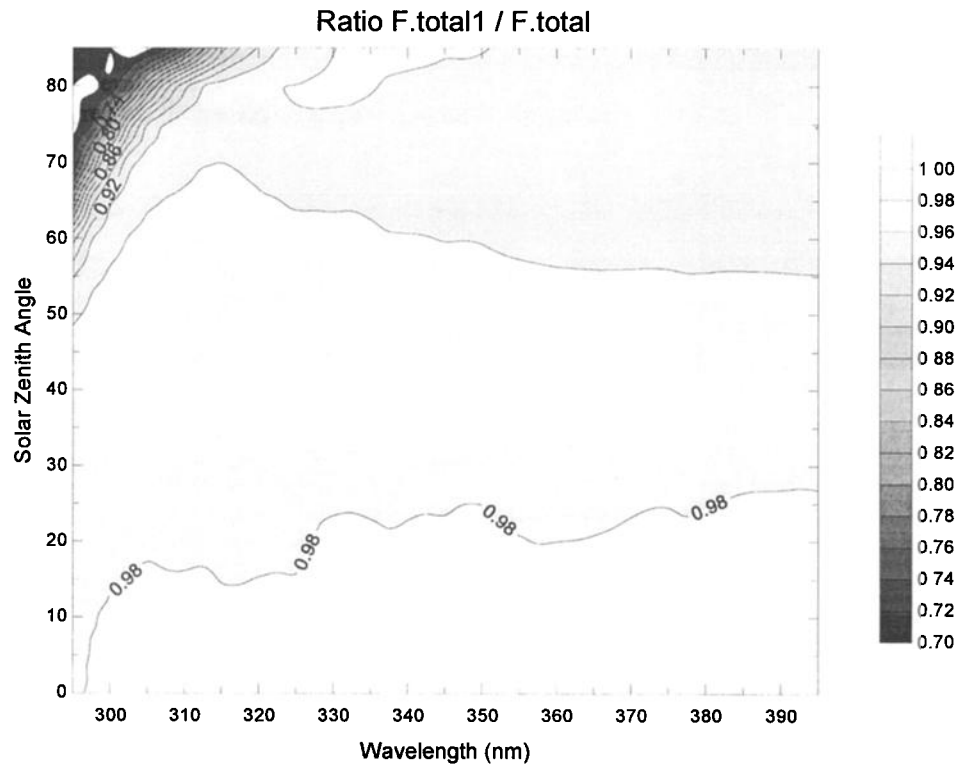

Figure 7b. Total irradiance ratio at sea level for case 1.

such as the pressure vertical distribution and ozone concentrations correspond to the summer midlatitudes atmospheric model [*Anderson*, 1987]. The Rayleigh scattering contribution has been evaluated by the *WMO* [1980] expression, pressure corrected. In this simulation for a clean situation the aerosol vertical distribution has been modeled following the *WCRP* [1986] MAR-I model for the troposphere, the background stratosphere aerosols for the stratosphere, and the upper atmospheric aerosols for the upper atmospheric layers.

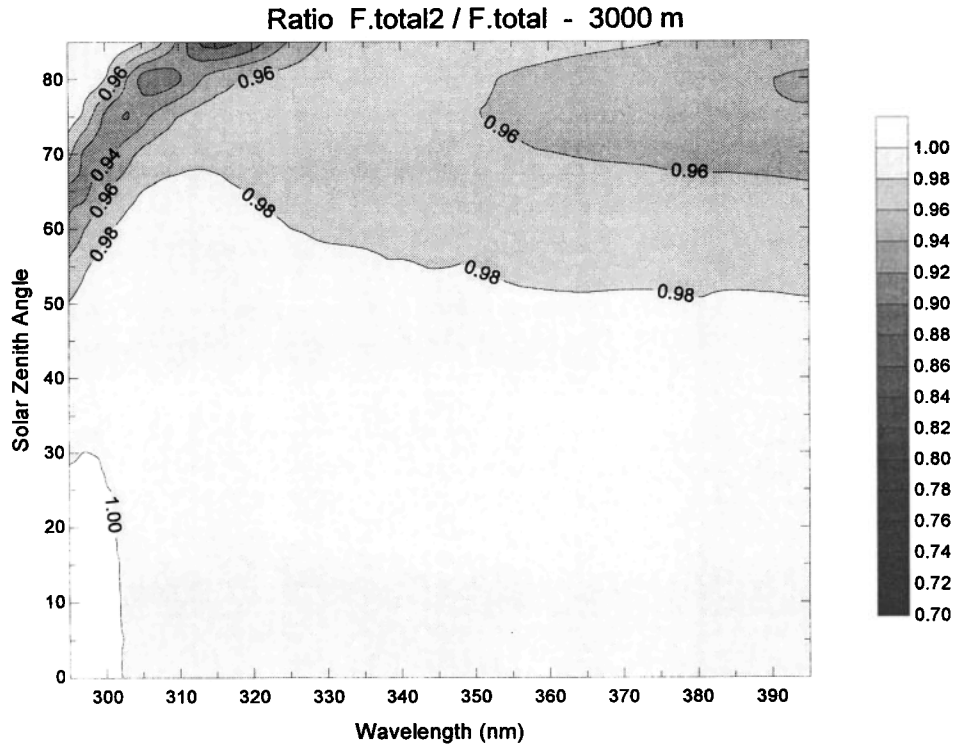

Figure 7c. Total irradiance ratio at 3000 m for case 2.

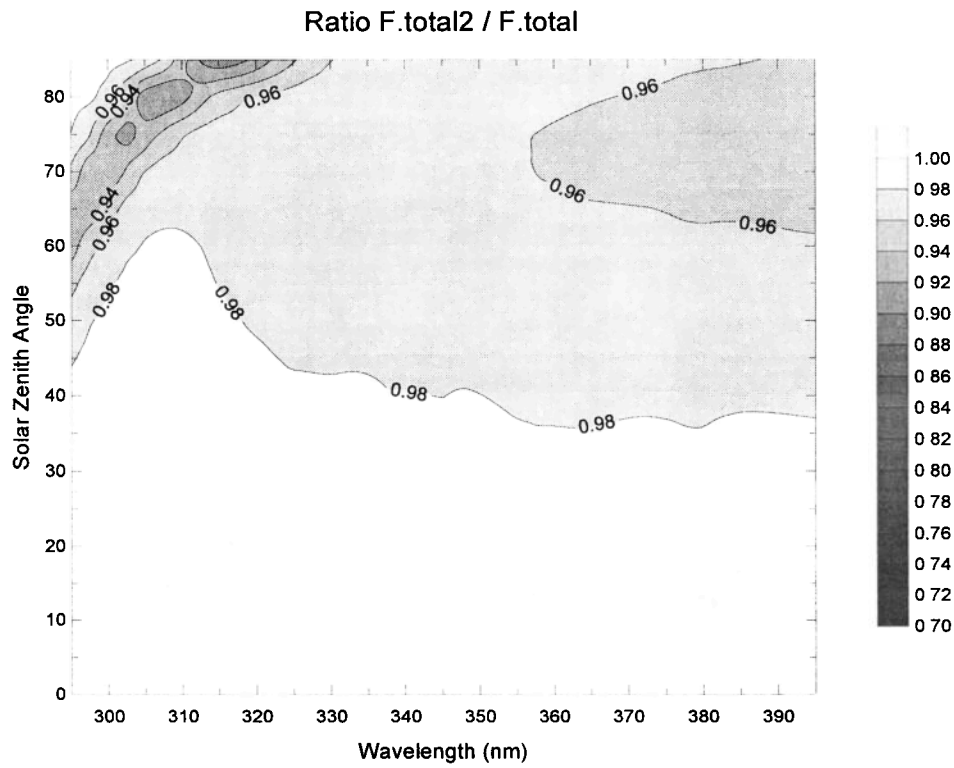

Figure 7d. Total irradiance ratio at sea level for case 2.

The presence of mineral dust in this atmospheric scheme has been modeled considering the next three patterns. The case 1 corresponds to the situation in which the desert dust is present below 1500 m (above sea level (asl)). This altitude is selected because is possible for the transport of dust in the atmosphere [*Husar et al.*, 1997]. In case 2 the desert aerosol plume is concentrated between 1500 and 6000 m (asl). In case 3 we consider that the mineral aerosols are distributed between sea level and 6000 m (asl). *Tegen and Fung* [1994] have shown that the greater mineral dust particle percentage is located in this layer. The layer is called the Saharan aerosol layer (SAL) in the African and North Atlantic subtropical

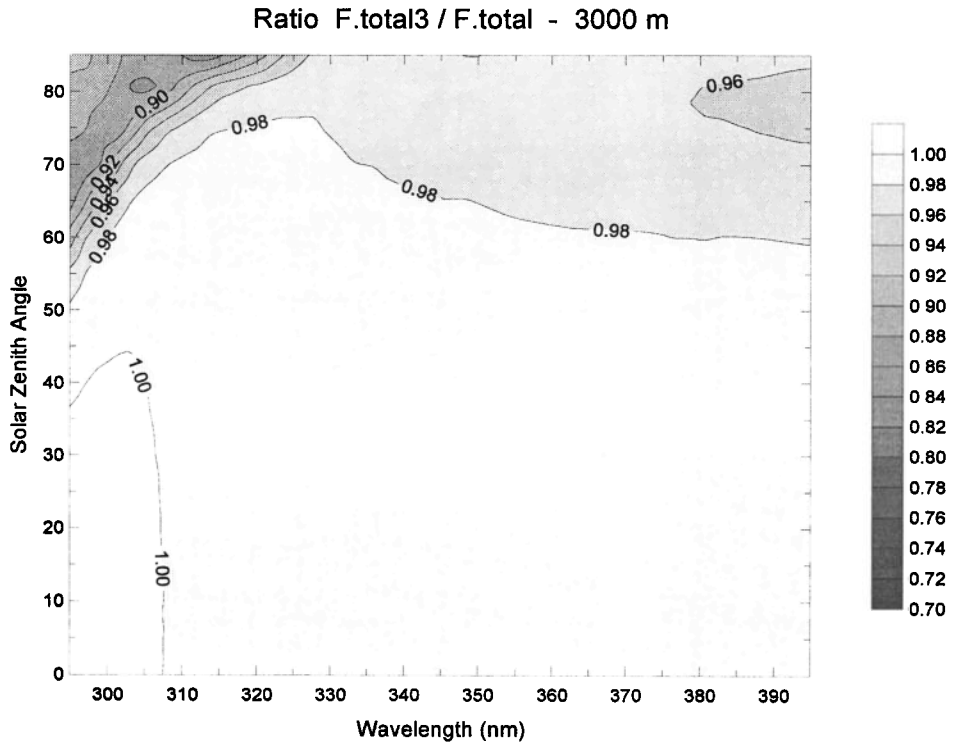

Figure 7e. Total irradiance ratio at 3000 m for case 3.

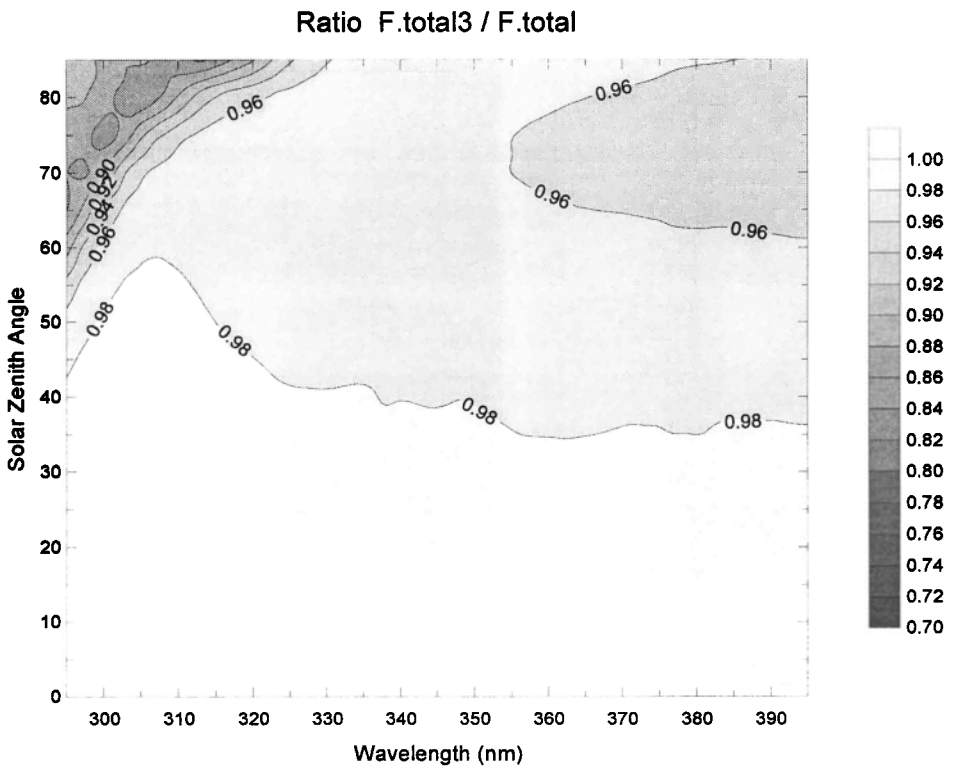

Figure 7f. Total irradiance ratio at sea level for case 3.

region. Figure 6 shows the aerosol optical depth values for the 20 layers in which the atmosphere has been divided for the three cases.

The aerosol optical depth considered for the clean situation is 0.2 at 550 nm, a limit value that has been found in remote ocean areas [*Husar et al.*, 1997]. The mineral dust optical depth in the three cases is 0.3 (at 550 nm), which is an average value in zones affected frequently by mineral dust invasions [*Díaz et al.*, 1994; *Tegen and Lacis*, 1996].

4. Discussion

In Figures 7a-7f we can see the ratios of the total spectral irradiance with the presence of mineral dust (F.total1, F.total2,

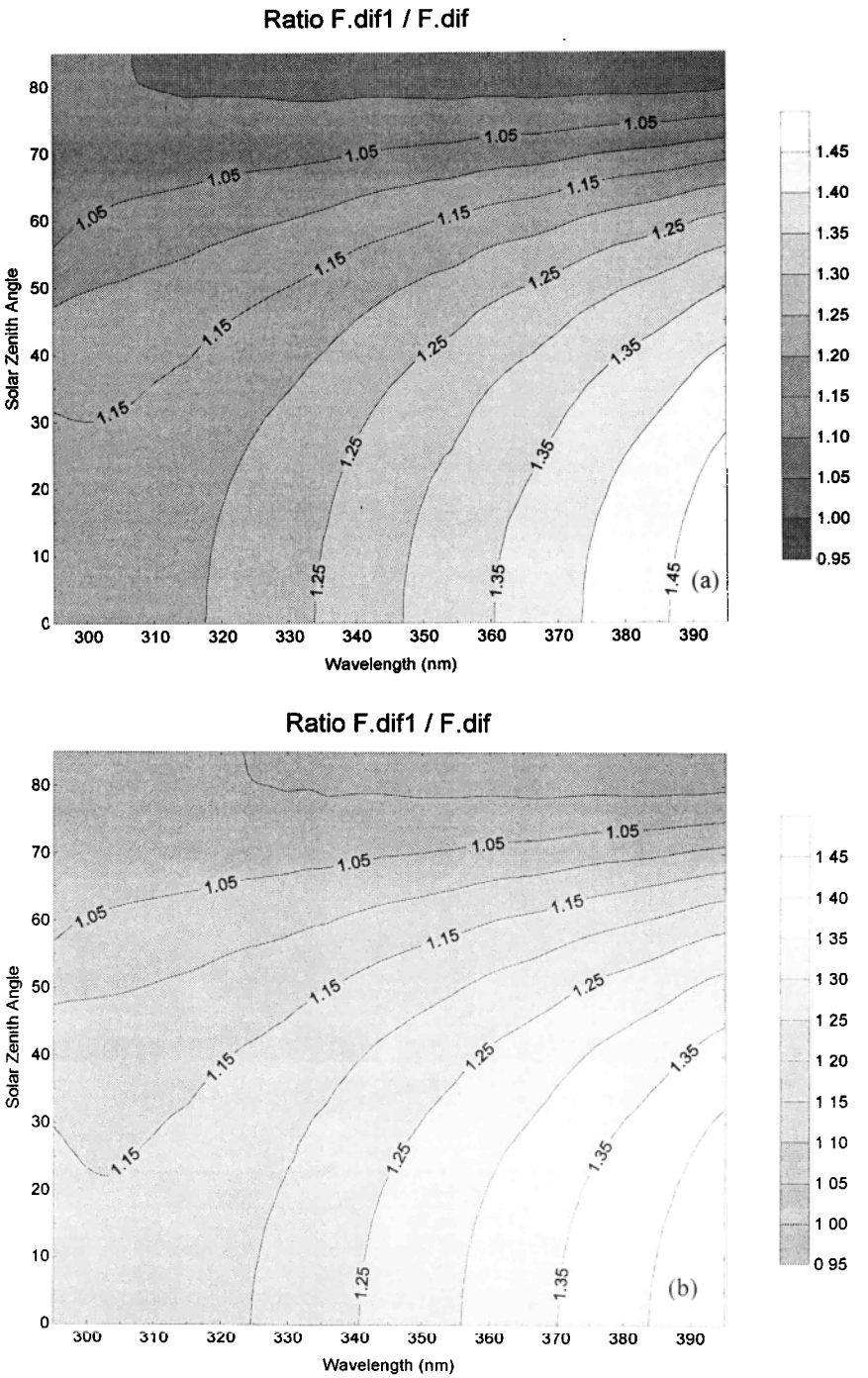

Figure 8. Diffuse irradiance ratio at sea level for summer midlatitudes atmosphere with (a) maritime aerosol vertical size distribution and (b) a continental aerosol vertical size distribution. The dust is present between 6000 m and sea level.

and F.total3) to those calculated during clean situations, F.total. They have been computed for the three scenarios above described both at the altitude of 3000 m (top panel) and at sea level (bottom). These ratios have been calculated in the wavelength range from 290 to 400 nm and for the solar zenith angle range from 0° to 85°

From Figure 7a we can see that the spectral irradiance at 3000 m has no significant differences with regard to clean situations when the dust is arriving below 1500 m (asl). There is an exception for the region of the shortest wavelengths and very high solar zenith angle. In Figure 7b the ratio at sea level shows a decrease of the total UV irradiance when the dust is present in the atmosphere lower levels. This reduction is slightly dependent on wavelength up to 310 nm and is more important at the shortest wavelengths. For a given wavelength there is a reduction in this ratio with the solar zenith angle (SZA). Thus we can see how this ratio is 0.98 for a SZA between 0° and 20°, whereas at 50°, it has a value of 0.94. This reduction is due to the increase in the path length.

In Figures 7c and 7d for case 2, where the dust is located

between 1500 m and 6000 m (asl), we can observe a quite different pattern from the above description. It is clear from Figure 7c to the altitude of 3000 m the quasi-constant value of the ratio up to 50° of SZA, with a ratio value of 0.98. At sea level (Figure 7d), a very similar behavior is observed to that found at 3000 m, although the isolines appear displaced to a smaller SZA. So the ratio value of 0.98 is located at 40° SZA.

Finally, Figures 7e and 7f show the third case, with the dust distributed between 6000 m and sea level. They show a very similar pattern as in case 2 at both altitudes. For the ratio at 3000 m the isoline of 0.98 is now located at 60° SZA. At sea level both figures for cases 2 and 3 look very similar.

To study the sensitivity of the UV levels to different background aerosol size distributions with the presence of mineral dust, we have simulated these radiation levels at the ground for a summer midlatitudes atmosphere with several standard aerosol vertical size distributions. In Figure 8 we can see the ratios of the diffuse radiation with dust to the calculated values without dust. The background tropospheric aerosol size distributions are the maritime model (Figure 8a) and the continental model (Figure 8b). The stratosphere and the upper levels of the atmosphere contain the same distribution as in the three cases previously studied. The shape of this curve is very similar to that obtained formerly. The similitude between both figures is evident, although the maritime model presents a greater diffuse radiation to the same wavelengths and SZA.

5. Conclusion

From Figures 7a to 7e we can see that for the same mineral dust optical depth, the total spectral irradiance depends on the dust vertical distribution. This can be shown not only at 3000 m but also at sea level. So, when dust is transported below 1500 m (case 1) the spectral irradiance at 3000 m does not change significantly, whereas at sea level the reduction in the spectral total energy levels is between 2 and 4%, even for low solar zenith angles (SZA) On the other hand, if the desert dust is transported between 6000 m and 1500 m (case 2), we have computed a similar modification in both levels. In this case, for the same SZA, the reduction is more important at sea level (2% at 40° SZA) than at 3000 m (2% at 55° SZA). If we compare the results at sea level for cases 1 and 2, we can observe that for the same SZA the differences do not exceed 2%. Finally, when the dust is distributed between 6000 m and sea level (case 3), it could be considered like an intermediate case between the first and the second one. On the other hand, we have observed that the diffuse UV levels depend not only on the vertical dust distribution but also on the background aerosol distribution. Thus we can see in Figures 8a and 8b how to the same mineral dust aerosol optical depth and vertical distribution the diffuse UV levels are different for a maritime aerosol model and for a continental aerosol distribution. For the same SZA and wavelength the differences can be of about 5%. From all this, we can conclude that to fully study the radiative forcing in the UV solar wavelengths, it is necessary to know the vertical dust concentration and not only the total concentration.

Acknowledgments. This work has been supported by the CICYT (Comisión Interministerial de Ciencia y Tecnología- Spanish Government) under contract CLI97-0453 and the Gobierno Autónomo de Canarias by contract 4/95. We want to thank A. Mujica for his help in writing this paper.

References

Amato, U.. V. Cuomo, F. Fontana, M. Macchiato, and C Serio, Inference of atmospheric aerosol size distribution from ground measurements of solar radiation, in *Aerosols and Climate*, edited by Peter V. Hobbs and M.P. McCormick, pp. 101-116, A. Deepak, Hampton, Va., 1988.

Anderson, G. P., S. A. Clough, F. X. Kneizys, J. H. Chetwynd, and E. P. Shettle, AFGL Atmospheric constituent profile (0-120 km), *AFGL-TR-86-0110 (OPI)*, Hascom, Air Force Base, Mass., 1987.

Arimoto, R., R. A. Duce, B. J Ray, W°. G. Ellis Jr., J. D. Cullen, and J. T. Merrill, Trace elements in the atmosphere over the North Atlantic, *J. Geophys. Res., 100*, 1199-1213, 1995.

Box, M. A., and A. Deepak, Atmospheric scattering corrections to solar radiometry, *Appl. Opt., 12*, 1941-1949, 1979.

Díaz, J. P., F. J. Expósito, and A. Díaz, Measurements of aerosols from Tenerife, in *Air Pollution '94*, edited by J. M. Baldasano, C. A. Brebbia, H. Power and P. Zannetti, pp. 400-408, Comput. Mech., Southampton, England, 1994.

Dutton, E. G.. R. Patrick, S. Ryan, and J. J. DeLuisi, Features and effects of aerosol optical depth observed at Mauna Loa, Hawaii: 1982-1992, *J. Geophys. Res., 99*, 8295-8306, 1994.

Expósito, F. J., J. P. Díaz, M. Arbelo, F. Herrera, and J C. Guerra, First intercomparison between the AOD data obtained by the NOAA satellites and the Optronic OL752 spectroradiometer in the Canary Islands, *Int. J. Remote Sens., 18* (10), 2247-2252, 1997.

Forster, P. M , Modeling ultraviolet radiation at the Earth's surface, part I, The sensitivity of ultraviolet irradiances to atmospheric changes, *J. Appl. Meteorol., 34*, 2412-2425, 1995.

González-Jorge, H., and J. Ogren, Sensitivity of retrieved aerosol properties to assumptions in the inversion of spectral optical depths, *J Atmos. Sci., 53*, 3669-3683, 1996.

Heintzenberg, J., H. Müller, H. Quenzel, and E. Thomalla, Information content of optical data with respect to aerosol properties: Numerical studies with a randomize minimization-search-technique inversion algorithm, *Appl. Opt., 20* (8), 1308-1315, 1981.

Herman, B. M, M. A. Box, J. Reagan, and C. M. Evans, Alternate approach to the analysis of solar photometer data, *Appl. Opt., 20* (17), 2925-2928, 1981.

Herman, J. R., P. K. Barthia, O. Torres, C. Hsu, C. Setfor, and E. Celarier, Global distribution of UV-absorbing aerosols from Nimbus 7/TOMS data, *J. Geophys. Res., 102*, 16,911-16,922, 1997

Husar, R. B., L. L. Stowe, and J. M. Prospero, Characterization of atmospheric aerosols over the oceans with the NOAA AVHRR optical thickness operational product, *J. Geophys. Res , 102*, 16,889-16,909, 1997.

Iqbal, M., *An Introduction to Solar Radiation*, Academic, San Diego, Calif., 1983.

Kahn, R., R. West, D. McDonald, and B. Rheingans, Sensitivity of multiangle remote sensing observations to aerosol sphericity, *J. Geophys. Res., 102*, 16,861-16,870, 1997.

Kiehl, J. T., and B. P. Briegleb, The relative roles of surface aerosol and greenhouse gases in climate forcing, *Science, 260*, 311-314, 1993.

King, M. D., D. M. Byrne, B.M. Herman, and J. A. Reagan, Aerosol size distributions obtained by inversion of spectral optical depth measurements, *J. Atmos. Sci., 35*, 2153-2167, 1978.

Lacis, A. A., and M. I. Mishchenko, Climate forcing, climate sensitivity and climate response: A radiative modeling perspective on atmospheric aerosols, in *Aerosol Forcing of Climate*, edited by R. J. Charlson and J. Heitzenberg, pp. 11-42, John Wiley, New York, 1995.

Longtin, D. R , E. P. Shettle, J. R. Hummel, and J. D. Pryce, A desert aerosol model for radiative transfer studies, in *Aerosols and Climate*, edited by Peter V. Hobbs and M.P. McCormick, pp 261-269, A. Deepak, Hampton, Va., 1988.

Mishchenko, M. I., A. A. Lacis, B. E. Carlson, and L. D. Travis, Nonsphericity of dust-like tropospheric aerosols: Implications for aerosol remote sensing and climate modeling, *Geophys. Res. Lett., 22*, 1077-1080, 1995.

Mishchenko, M. I., L. D. Travis, R. A. Kahn, and R. A. West, Modeling phase functions for dust-like tropospheric aerosols using a shape mixture of randomly oriented polydisperse spheroids, *J. Geophys. Res., 102*, 16,831-16,847, 1997.

Patterson, E. M., D. A. Gillette, and B. H. Stockton, Complex index of refraction index between 300 and 700 nm for Saharan aerosols, *J. Geophys. Res.*, *82*, 3153-3160, 1978.

Penner, J. E., R. E. Dickinson, and C. A. O'Neill, Effects of aerosols from biomass burning in the global radiation budget, *Science*, *256*, 1432-1433, 1992.

Porter, J. N., *Measuring Aerosol Optical Depth from Satellite: Aerosol Measurements and Models*, Ph.D. dissertation, Univ. of Hawaii, Hawaii, 1993.

Prospero, J. M., Saharan dust transport over the North Atlantic Ocean and Mediterranean: An overview, in *The Impact of Desert Dust Across the Mediterranean*, edited by S. Guerzoni and R. Chester, pp. 133-151, Kluwer Acad., Norwell, Mass., 1996a.

Prospero, J. M., The atmospheric transport of particles to the ocean, in *Particle Flux in the Ocean*, edited by V. Ittekkott, S. Honjo, and P. J. Depetris, pp. 19-52, *SCOPE Rep. 57*, John Wiley, New York, 1996b.

Reagan, J. A., L. W. Thomason, B. M. Herman, and J. M. Palmer, Assessment of atmospheric limitations on the determination of the solar spectral constant from the ground-based spectroradiometer measurements, *IEEE Trans. Geosci. Remote Sens.*, *GE-24* (2), 258-266, 1986.

Russell, P. B., et al., Pinatubo and pre-Pinatubo optical depth spectra: Mauna Loa measurements, comparisons, inferred particle size distributions, radiative effects, and relationship to lidar data, *J. Geophys. Res.*, *98*, 22,969-22,985, 1993.

Sokolik, I. N., and O. B. Toon, Direct radiative forcing by anthropogenic airborne mineral aerosols, *Nature*, *381*, 681-683, 1996.

Stamnes, K., S. C. Tsay, W. Wiscombe, and K. Jayaweera, Numerically stable algorithm for discrete-ordinate-method radiative transfer in multiple scattering and emitting layered media, *Appl. Opt.*, *27* (12), 2502-2509, 1988.

Taylor, K. E., and J. E. Penner, Response of climate system to atmospheric aerosols and greenhouse gases, *Nature*, *369*, 734-737, 1994.

Tegen, I., and I. Fung, Modeling of mineral dust in the atmosphere: Sources, transport, and optical thickness, *J. Geophys. Res.*, *99*, 22,897-22,914, 1994.

Tegen I., and A. A. Lacis, Modeling of particle size distribution and its influence on the radiative properties of mineral dust aerosol, *J. Geophys. Res.*, *101*, 19,237-19,244, 1996.

Tegen, I., A. A. Lacis, and I. Fung, The influence on climate forcing of mineral aerosols from disturbed soils, *Nature*, *380*, 419-422, 1996.

Thomason, L. W., B. M. Herman, and J. A. Reagan, The effect of atmospheric attenuators with structured vertical distributions on air mass determinations and Langley plot analyses, *J. Atmos. Sci.*, *40*, 1851-1854, 1983.

Wiscombe, W., *Mie Scattering Calculations; Advances in Technique and Fast, Vector-Speed Computer Codes*, U.S. Nat. Cent. for Atmos. Res., Boulder, Colo., 1980.

World Climate Research Program (WCRP) (IAMAP Radiation Commission). A preliminary cloudless atmosphere for radiation computation, *WCP-112*, *WMO/TD-24*, 55 pp., WMO, Geneva, 1986.

World Meteorological Organization (WMO), Report of Second WMO Expert Meeting on Turbidity Measurements, Boulder, Colorado, Geneva, 1980.

West, R. A., L. R. Doose, A. M. Eibl, and M. G. Tomasko, Laboratory measurements of mineral dust scattering phase function and linear polarization, *J. Geophys. Res.*, *102*, 16,871-16,881, 1997.

V. Carreño, J. P. Díaz, F. J. Expósito, and C. J. Torres, University of La Laguna, Department of Physics, A/Astrofísico Francisco Sánchez, s/n, 38200 La Laguna, Santa Cruz de Tenerife, Canary Islands, Spain. (jpdiaz@ull.es)

A. Redondas, Instituto Nacional de Meteorología, Izaña GAW Station, C/San Sebastián, 77, 38071 Santa Cruz de Tenerife, Canary Islands, Spain.

(Received June 11, 1999; revised September 29, 1999;
accepted October 5, 1999.)